Acta Cryst. (1996). B52, 251–259

Theoretical Study of the Deformation Densities of *d* Electrons in $K_2[PdCl_6]$ and $K_2[PtCl_6]$ Crystals

YOSHIKO SAKAI, TAKASHI OSHIBE AND EISAKU MIYOSHI

Department of Applied Physics, Faculty of Engineering, Kyushu University Ropponmatsu, Fukuoka 810, Japan

(Received 26 July 1995; accepted 29 August 1995)

Abstract

Aspherical distributions of the *d* electrons in dipotassium palladium hexachloride, $K_2[PdCl_6]$, and dipotassium platinum hexachloride, $K_2[PtCl_6]$, crystals were analyzed by theoretical calculations. Hartree–Fock and configuration interaction calculations were performed for $[PdCl_6]^{2-}$ and $[PtCl_6]^{2-}$ with and without taking into account the Madelung potentials, using a model potential method. The major relativistic effects were incorporated in the model potentials for Pd and Pt. The deformation-density maps calculated were similar to those given by the X-ray diffraction method. The theoretical result suggested that the positive peaks on the threefold axes and the negative peaks on the metal–Cl bond axis correspond to the excess *d* electrons (4*d* of Pd and 5*d* of Pt) in the t_{2g} (d_{xy}, d_{xz}, d_{yz}) orbitals and the electron deficiency in the e_g $(d_{z^2}, d_{x^2-y^2})$ orbitals, respectively. The positive and negative peak heights were calculated to be $+1.8$ and $-0.8\,e\,Å^{-3}$ for $[PdCl_6]^{2-}$ and $+1.2$ and $-0.6\,e\,Å^{-3}$ for $[PtCl_6]^{2-}$. The effective charges and effective radii of Pd and Pt, and the number of electrons in the t_{2g}, e_g and t_{1u} orbitals, were calculated by direct integration. The effects of the Madelung potential and electron correlation on the charge distributions of $[PdCl_6]^{2-}$ and $[PtCl_6]^{2-}$ were also analyzed.

1. Introduction

The aspherical *d*-electron distribution in 3*d* and 4*d* transition-metal complexes has been widely studied by the X-ray diffraction method (Stevens & Coppens, 1976; Coppens & Hall, 1982; Toriumi & Saito, 1983). However, the 5*d* transition-metal complexes have been scarcely studied because of the difficulty in detecting 5*d* electrons due to the strong absorption effect and a small valence/total electron ratio (Stevens & Coppens, 1976). Ohba *et al.* successfully detected the aspherical charge distribution in $K_2[PtCl_4]$ (Ohba, Sato, Saito, Ohshima & Harada, 1983) and $K_2[PtCl_6]$ (Ohba & Saito, 1984) crystals at 300 K. Takazawa Ohba & Saito (1988) reported the results for $K_2[PdCl_4]$ and $K_2[PdCl_6]$ crystals at 120 K using Mo $K\alpha$ radiation. Extensive studies on 5*d* transition-metal complexes, $K_2[MCl_6]$ (M = Re, Os, Pt) and $K_2[PtCl_4]$, were performed at 120 K using Ag $K\alpha$ radiation by Takazawa, Ohba, Saito & Sano (1990). They also reported data using Mo $K\alpha$ radiation for $K_2[PtCl_6]$ and $K_2[PtCl_4]$. They obtained deformation-density maps to visualize the aspherical *d*-electron distributions for these crystals and estimated the positive and negative peak heights of the deformation density. The effective radii and effective charge of the central metal atoms were also estimated (Takazawa *et al.*, 1988; Takazawa *et al.*, 1990).

To date, theoretical studies using *ab initio* calculations to examine the aspherical *d*-electron distribution have been reported only for 3*d* transition-metal complexes (Johansen, 1976; Sano, Hatano, Kashiwagi & Yamatera, 1981; Sano, Kashiwagi &Yamatera, 1982). The deformation-density maps for $[PdCl_6]^{2-}$ and $[PtCl_6]^{2-}$ were calculated by the discrete-variational $X\alpha$ (DV-$X\alpha$) method (Takazawa *et al.*, 1990). Although their maps supported qualitatively the excess electron density on the threefold axes observed for $K_2[PdCl_6]$ and $K_2[PtCl_6]$, details of the electron density on the metal–Cl bond axis were not described clearly. It is not easy to perform *ab initio* calculations on 5*d* transition-metal complexes, because the systems contain a large number of electrons and the relativistic effects must be taken into account for 5*d* metal atoms.

The development of effective core potential (ECP) methods has enabled us to more easily examine systems containing heavier atoms. A model potential (MP) method developed by Sakai *et al.* (Sakai & Huzinaga, 1982*a*,*b*; Sakai, Miyoshi, Klobukowski & Huzinaga, 1987*a*,*b*), which is a type of ECP method, has been successfully applied to a number of molecular calculations (Sakai & Miyoshi, 1987, 1988; Miyoshi & Sakai, 1988*a*,*b*, and references therein; Miyoshi, Sakai & Katsuki, 1991, and references therein). In the present study, we analyzed the aspherical distributions of the 4*d* and 5*d* electrons in $K_2[PdCl_6]$ and $K_2[PtCl_6]$ crystals by theoretical calculations using the MP method. Relativistic MPs were used for the Pd and Pt atoms (Sakai *et al.*, 1987*b*). Hartree–Fock (HF) and singly and doubly excited configuration interaction (SDCI) calculations were performed for $[PdCl_6]^{2-}$ and $[PtCl_6]^{2-}$. We used embedded cluster models to account for the Madelung potentials due to the surrounding ions, in addition to the bare cluster models. Deformation-density maps were

calculated to reproduce the positive and negative peaks of the deformation densities observed (Takazawa *et al.*, 1988; Takazawa *et al.*, 1990) on the threefold axis and the metal–Cl bond axis, respectively. The effective charges and effective radii of Pd and Pt, and the number of electrons in the t_{2g}, e_g and t_{1u} orbitals were also calculated by direct integration.

2. Computational details

HF and CI calculations were performed for $[PdCl_6]^{2-}$ and $[PtCl_6]^{2-}$ using the model potential method (Sakai & Huzinaga 1982*a*,*b*; Sakai *et al.*, 1987*a*,*b*). The M—Cl distances for M = Pd and Pt were fixed at the observed values of 4.3641 a.u. (Takazawa *et al.*, 1988) and 4.3774 a.u. (Takazawa *et al.*, 1990), respectively. The *spd*-MP sets (Sakai *et al.*, 1987*b*) were used for Pd and Pt atoms, in which *nd*, *np* and $(n+1)s$ electrons were treated explicitly and the other electrons are replaced by the MP's. The major relativistic effects were incorporated into the MP's and basis sets at the level of Cowan and Griffin's quasi-relativistic HF method (Cowan & Griffin, 1976). Two *p*-type polarization functions (Sakai *et al.*, 1987*a*) were added to the MP basis sets for Pd and Pt atoms. For Cl atoms we examined both the all-electron (AE) and MP calculations to verify the validity of using the MP. In the MP set for Cl (Sakai & Miyoshi, unpublished), only the 3*s* and 3*p* electrons were treated explicitly. The AE basis set for Cl was taken from the work of Huzinaga, Andzelm, Klobukowski, Radzio-Andzelm, Sakai & Tatewaki (1984). All the basis sets were expanded in terms of Gaussian-type functions (GTF's). The *s*-, *p*- and *d*-type primitive GTF's (*s*/*p*/*d*) were contracted as follows:

Pd : MP(611/411*1*/3111$^+$),
Pt : MP(611/511*1*/3111),
Cl : AE(4321/4111),
Cl : MP(31/311$^+$),

where 1* and 1$^+$ indicate one *p*-type polarization function and one diffuse function, respectively.

In addition to the calculations on bare $[MCl_6]^{2-}$ ion clusters, we also considered an embedded cluster model in which the $[MCl_6]^{2-}$ ion was located at the center of an ionic crystal composed of point charges. The surrounding point charges were determined as follows: The charge of the K^+ ion was fixed to be +1 e (Ohba & Saito, 1984). By a preliminary calculation on $[MCl_6]^{2-}$ we obtained the effective charges of +2.02 e and +2.38 e for Pd and Pt, respectively. The average value (+2.2 e) was assigned to M (Pd,Pt) and −0.7 e was assigned to Cl to keep the total charge in the unit cell neutral. The point charges were generated by the parallel transfer of the unit cell composed of point charges of +2.2 e, +1 e and −0.7 e assigned to M, K and Cl, respectively. The number of point charges considered was 13 874. We also assigned the charges of +2.2 e and −0.7 e for the reference atoms in the deformation densities for both $[PdCl_6]^{2-}$ and $[PtCl_6]^{2-}$. The charges are close to those, $Pt^{2.3+}$ and $Cl^{0.7-}$, used by Ohba & Saito (1984).

Four HF calculations (Calcs. 1–4) and an SDCI calculation (Calc. 5) were performed for $[PdCl_6]^{2-}$. These five methods are summarized as follows:

Calc. 1: HF, bare cluster model and AE for Cl;
Calc. 2: HF, embedded cluster model and AE for Cl;
Calc. 3: HF, bare cluster model and MP for Cl;
Calc. 4: HF, embedded cluster model and MP for Cl;
Calc. 5: SDCI, embedded cluster model and MP for Cl.

As shown in the next section, Calcs. 3 and 4 yield essentially the same results as Calcs. 1 and 2, respectively. Thus, only Calcs. 3, 4 and 5 were performed for $[PtCl_6]^{2-}$. The calculations were performed for the ground state, in which the electronic configuration in O_h symmetry is:

$$^1A_{1g} : (1-2)a_{1g}^2(1-2)e_g^4 1t_{1g}^6(1-2)t_{2g}^6(1-4)t_{1u}^6 1t_{2u}^6,$$

which does not include the core electrons of Cl atoms that are treated explicitly in Calcs. 1 and 2.

In the SDCI calculation (Calc. 5) all single and double excitations from the SCF configuration were considered by maintaining that the Pd 4*p*, Pt 5*p* and Cl 3*s* orbitals were always double occupied. To save configurational space, the configuration state functions (CSFs) were limited to the first-order interacting space (McLean & Liu, 1973; Tatewaki, Tanaka, Sasaki, Obara, Ohno & Yoshimine 1979). D_{2h} symmetry was used in the CI calculations. The number of CSFs was 125 488. The dimensions of CI were reduced to 11 739 and 11 998 for $[PdCl_6]^{2-}$ and $[PtCl_6]^{2-}$, respectively, by a second-order perturbation selection (Buenker & Peyerimhoff, 1974; Gershgorn & Shavitt, 1968) using an energy threshold of 5 μhartree. The HF and CI calculations were performed using the *JAMOL*4 (Kashiwagi, Obara, Takada, Sasaki & Miyoshi, 1979) and *MICA*3 (Murakami, Iwaki, Terashima, Shoda, Kawaguchi & Noro, undated) software programs, respectively.

3. Results and discussion

3.1. *Results for* $[PdCl_6]^{2-}$

Deformation-density maps were calculated using Calcs. 1–5. The map in the (110) plane given by the best calculation (Calc. 5) is shown in Fig. 1(*a*) as an example; all the other calculations yielded maps essentially the same as that in Fig. 1(*a*). The deformation densities were obtained by subtracting the densities of spherical atoms with specific charges, $\rho(Pd^{2.2+} + 6Cl^{0.7-})$, from the density of the cluster, $\rho([PdCl_6]^{2-})$,

while retaining the positions of the spherical atoms at the same locations as in $[PdCl_6]^{2-}$. The charge density $\rho(Pd^{2.2+})$ was calculated by giving 6 and 7.8 electrons to the $4p$ and $4d$ orbitals, respectively, which were determined for the $4p^64d^{10}$ configuration in the HF scheme. The $\rho(Cl^{0.7-})$ was also calculated by giving 2 and 5.7 electrons to the $3s$ and $3p$ orbitals determined for the F^- ion. The experimental deformation-density map obtained for $K_2[PdCl_6]$ at 120 K by Takazawa *et al.* (1988) is shown in Fig. 1(*b*). In both figures, contours are given at intervals of 0.2 e Å^{-3}. The solid and broken lines denote, respectively, the increase and decrease in the electron density upon formation of the cluster. Zero contours are given by dash–dotted lines. The asphericity of the $4d$ electron distribution is clearly seen in Fig. 1(*a*), which is quite similar to the experimental result shown in Fig. 1(*b*). In Fig. 1(*a*), positive peaks of +1.8 e Å^{-3} are located on the threefold axes at 0.45 Å from the Pd nucleus and negative peaks of −0.8 e Å^{-3} are located on the Pd—Cl bond axis at 0.51 Å from the Pd nucleus. The positive and negative peaks indicate an excess $4d$-electron population in the $t_{2g}(d_{xy}, d_{xz}, d_{yz})$ orbitals and a deficiency in the $e_g(d_{z^2}, d_{x^2-y^2})$ orbitals, respectively. Regarding the experimental map in Fig. 1(*b*) at 120 K, positive peaks of +1.4 (3) e Å^{-3} and negative peaks of −1.0 (2) e Å^{-3} are located at 0.51 and 0.48 Å, respectively, from the Pd nucleus (Takazawa *et al.*, 1988). To compare the experimental peak heights with calculated ones, the same charges should be assigned to the reference spherical atoms in both methods. Even if we used the same reference atoms, the peak heights of the experimental deformation density are expected to be smaller than those of the calculated ones, because the experimental peak heights depend on the temperature and the cutoff value $(\sin\theta/\lambda)_{max}$ in the Fourier summation (Takazawa *et al.*, 1988). It has been reported that peak heights decrease from +1.4 (3) e Å^{-3} at 120 K to +0.7 (2) e Å^{-3} at 300 K due to the thermal motion.

The effective charge and effective radius of Pd were obtained by direct integration (*JANIE*; Miyoshi, undated). The numerical integration was performed using Simpson's rule in many partitioned regions. The number of electrons in a sphere of radius r centered on Pd $C(r)$ and the radial charge distribution on a spherical surface of radius r, $D(r) = dC(r)/dr$, were calculated. In Fig. 2, the radial charge distributions, $D(r)$'s, obtained by Calc. 5 are plotted as a function of r. Using the MP method we can clearly see the fine structure of the valence electron distribution in the cluster, as shown in Fig. 2. The effective radius of Pd is defined as the r of the minimum $D(r)$ in the Pd—Cl bonding region (see Fig. 2). The effective charge of Pd is defined as the total charge (sum of the charges of nucleus and electrons) in a sphere of effective radius. The effective radius and effective charge given by Calcs. 1–5 are summarized in Table 1. The experimental data obtained from $K_2[PdCl_6]$ (Takazawa *et al.*, 1988) are given in Table 2, where the effective charge and effective radius of Pd were also estimated by direct integration of the electron densities. Table 1 shows that the calculations using the MP for Cl's yield essentially the same results as the calculations using the AE for Cl's (*cf.* Calc. 1 with Calc. 3 and Calc. 2 with Calc. 4). Calcs. 1–5 all give an almost equal effective radius of 2.26 a.u., which is close to the experimental value of 1.2 Å (2.3 a.u.). The effective charge of Pd is reduced by the effects of both the Madelung potential and electron correlation, as shown in Table 1. Calc. 5 gives an effective charge of +1.90 e. Thus, the effective charge of +1.16 (41) e estimated experimentally is smaller than the calculated value.

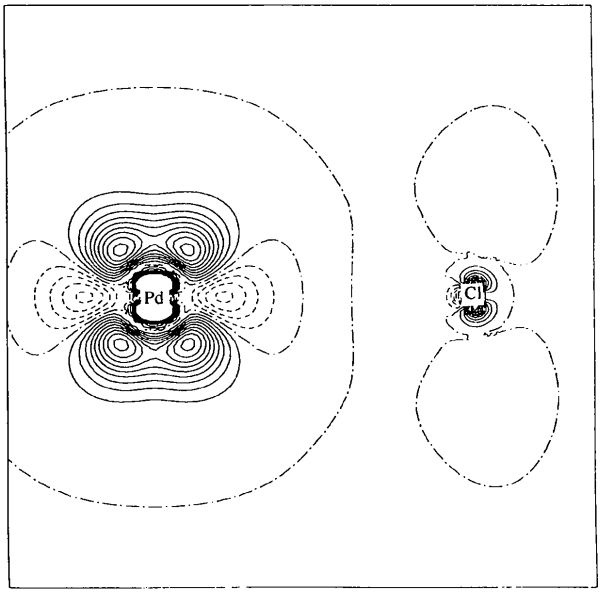

(*a*)

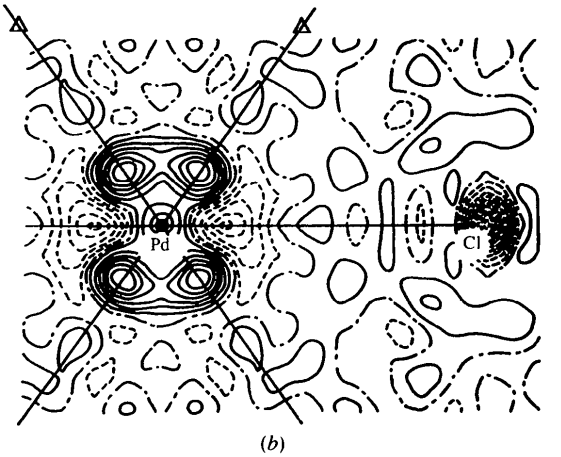

(*b*)

Fig. 1. (*a*) Deformation-density map in the (110) plane for $[PdCl_6]^{2-}$ given by Calc. 5. (*b*) Deformation-density map for $K_2[PdCl_6]$ at 120 K using Mo $K\alpha$ radiation (Takazawa *et al.*, 1988). Solid, broken and dash–dotted lines denote positive, negative and zero contours, respectively. Contours are drawn at intervals of 0.2 e Å^{-3}.

Table 1. *Effective charges and effective radii of Pd and Pt*

	Method of calculation*	Effective charge†	Effective radius (a.u.)
$[PdCl_6]^{2-}$	Calc. 1	+2.02 (13.98)	2.26
	Calc. 2	+1.97 (14.03)	2.25
	Calc. 3	+2.02 (13.98)	2.26
	Calc. 4	+1.96 (14.04)	2.26
	Calc. 5	+1.90 (14.10)	2.26
$[PtCl_6]^{2-}$	Calc. 3	+2.38 (13.62)	2.30
	Calc. 4	+2.32 (13.68)	2.30
	Calc. 5	+2.27 (13.73)	2.30

* See text for definition of Calcs. 1–5. † The number of electrons in a sphere of the effective radius is given in parentheses.

To examine the effects of the Madelung potential and electron calculation in detail, we depict the differences in $D(r)$s, $\Delta D(r)$ (Calc. 4 − Calc. 3) and $\Delta D(r)$ (Calc. 5 − Calc. 4), in Figs. 3(*a*) and (*b*), respectively. Note that the scale for $D(r)$ is much larger in Fig. 3 than in Fig. 2. In Fig. 3(*a*) the effect of the Madelung potential increases the electrons in the Pd—Cl bonding region (0.22 e) and just behind the Cl nuclei (0.09 e) by decreasing those in the outer region of the cluster (0.31 e). The effect of electron correlation also increases the electrons (0.06*e*) within the effective radius, as shown in Fig. 3(*b*).

The number of electrons in a sphere of radius r centered on Pd was also calculated for the t_{2g}, e_g and t_{1u} orbitals by direct integration. We determined the symmetry orbital radius of Pd, r_{so}, based on the minimum of the radial charge distribution for each symmetry orbital. The number of electrons in a sphere of r_{so} for the t_{2g}, e_g and t_{1u} orbitals is given in Table 3. Calcs. 1–5 all show essentially the same results. Table 3 shows that there are six electrons in the t_{2g} (d_{xy}, d_{xz}, d_{yz}) orbitals, whereas there are only two electrons in the e_g (d_{z^2}, $d_{x^2-y^2}$) orbitals. This result supports the asphericity of the deformation-density maps in Fig. 1. The six electrons in the t_{1u} orbitals correspond to the six electrons in the 4*p* orbitals of Pd. The symmetry orbital radii, r_{so}'s, given by Calc. 5, are 2.74, 2.38 and 2.02 a.u. for the t_{2g}, e_g and t_{1u} orbitals, respectively. Table 4 gives the number of electrons in a sphere of the effective radius (2.26 a.u.)

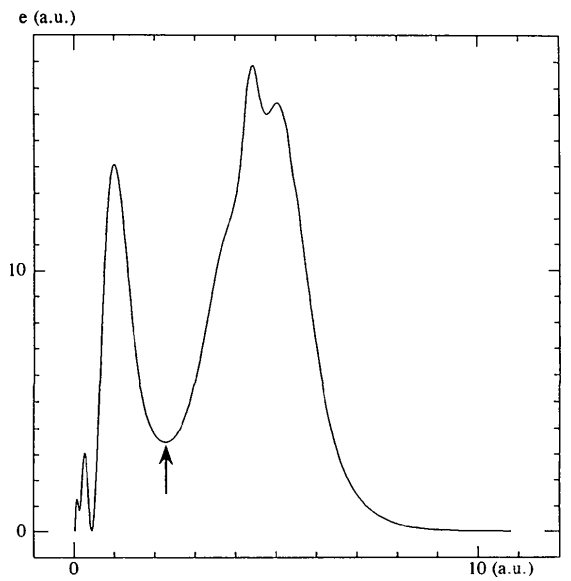

Fig. 2. Radial charge distribution, $D(r) = dC(r)/dr$, given by Calc. 5 for $[PdCl_6]^{2-}$. $C(r)$ is the number of electrons in a sphere of radius r centered on Pd. The arrow indicates the position of the effective radius.

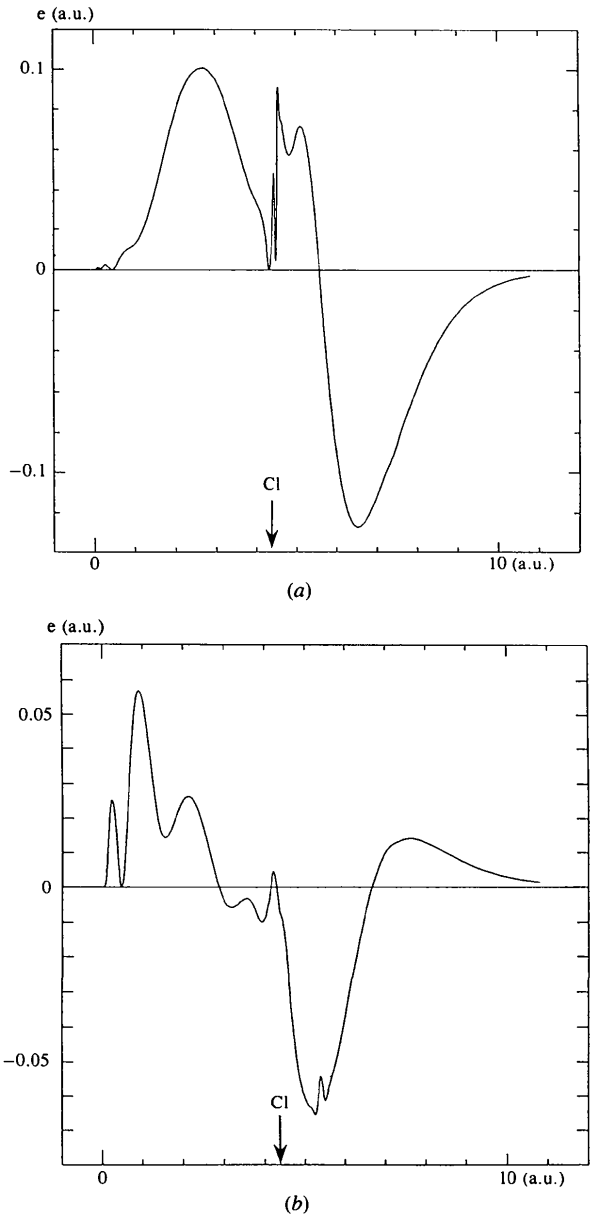

Fig. 3. (*a*) Difference in $D(r)$, $\Delta D(r)$ (Calc. 4 − Calc. 3), for $[PdCl_6]^{2-}$. (*b*) Difference in $D(r)$, $\Delta D(r)$ (Calc. 5 − Calc. 4), for $[PdCl_6]^{2-}$.

Table 2. *Effective charges, number of electrons in t_{2g} and e_g orbitals, M—Cl distances and effective radii for $K_2[MCl_6](M = Pd, Pt)$ obtained experimentally*

	Effective charge	Number of electrons t_{2g}	e_g	$(t_{2g}+e_g)$	M—Cl distance (Å)	Effective radius (Å)
$K_2[PdCl_6]$*	+1.16 (41)	6.14 (8)	1.89 (7)	8.03 (10)	2.3094	1.2 (2.3 a.u.)
$K_2[PtCl_6]$ (I)†	+1.6 (3)	6.0§	2.97 (15)	8.97 (15)	2.3164 (8)	1.2
$K_2[PtCl_6]$ (II)‡	+1.3 (8)	6.0§	2.12 (12)	8.12 (12)	2.3152 (5)	1.2

* See Takazawa *et al.* (1988), Mo $K\alpha$ data, at 120 K. † See Takazawa *et al.* (1990), Ag $K\alpha$ data, at 120 K. ‡ See Takazawa *et al.* (1990), Mo $K\alpha$ data, at 120 K. § These values were fixed.

Table 3. *Symmetry orbital radius (r_{so}) and number of electrons in a sphere of r_{so} for the t_{2g}, e_g and t_{1u} orbitals*

Cluster	Method*	t_{2g} Electrons	t_{2g} r_{so} (a.u.)	e_g Electrons	e_g r_{so} (a.u.)	t_{1u} Electrons	t_{1u} r_{so} (a.u.)
$[PdCl_6]^{2-}$	Calc. 1	5.98	2.84	1.97	2.34	6.07	2.01
	Calc. 2	5.95	2.84	2.06	2.37	6.07	2.01
	Calc. 3	5.96	2.84	1.98	2.34	6.07	2.02
	Calc. 4	5.95	2.84	2.06	2.36	6.07	2.01
	Calc. 5	5.88	2.74	2.18	2.38	6.08	2.02
$[PtCl_6]^{2-}$	Calc. 3	5.93	2.94	1.90	2.36	6.05	2.06
	Calc. 4	5.92	2.93	1.97	2.37	6.06	2.06
	Calc. 5	5.84	2.82	2.09	2.40	6.06	2.05

* See text for definition of Calcs. 1–5.

for the t_{2g}, e_g, t_{1u} and a_{1g} orbitals. By comparing Table 3 with Table 4 we find that a significant amount of 4*d* electrons (~0.4 electrons) in the t_{2g} orbitals are distributed outside the effective radius, whereas most of the 4*d* electrons in the e_g orbitals are distributed within the effective radius. The effects of both the Madelung potential and electron correlation decrease the electrons in the t_{2g} orbitals and increase those in the e_g orbitals, which strengthens the Pd—Cl bonds. Contributions of 5*s* and 5*p* electrons to the t_{1u} and a_{1g} orbitals, respectively, are also observed in Table 4.

We will now discuss the nature of the molecular orbitals which contain Pd 4*d*- and 5*s*-orbital components. The $2a_{1g}$ orbital, which consists mainly of Cl 3*p* orbitals, is slightly bound with the Pd 5*s* orbital. The $1t_{2g}$ orbitals are strongly localized on the Pd atom and the $2t_{2g}$ orbitals are weakly antibonding. In contrast to these orbitals, the $2e_g$ orbitals have strong bonding characteristics, as shown in Fig. 4(*a*), which presents the $2e_g$ orbital in the *xz* plane as an example. Therefore, the $[MCl_6]^{2-}$ ion has a covalent bonding character through the $2e_g$ orbitals. Fig. 4(*b*) shows the $3e_g$ orbital, which is the lowest unoccupied orbital (LUMO), with an antibonding character. The aspherical *d*-electron distribution is reflected in a deficiency of 3*d* electrons in this LUMO.

3.2. *Results for $[PtCl_6]^{2-}$ and comparison with $[PdCl_6]^{2-}$*

Calcs. 3, 4 and 5 were also performed for $[PtCl_6]^{2-}$. The deformation-density map in the (110) plane for $[PtCl_6]^{2-}$ given by Calc. 5 is depicted in Fig. 5(*a*). The charges of spherical atoms were taken to be $Pt^{2.2+}$ and $Cl^{0.7-}$, which were the same as those for $[PdCl_6]^{2-}$. The aspherical distribution of 5*d* electrons for $[PtCl_6]^{2-}$ in Fig. 5(*a*) is very similar to that of 4*d* electrons for $[PdCl_6]^{2-}$ shown in Fig. 1(*a*). The map obtained experimentally for $K_2[PtCl_6]$ at 120 K using Ag $K\alpha$ radiation (Takazawa *et al.*, 1990) is shown in Fig. 5(*b*). Takazawa *et al.* (1990) have reported both Ag $K\alpha$ and Mo $K\alpha$ data for $K_2[PtCl_6]$. We compared our results with their Ag $K\alpha$ data, since the error of the effective charge is smaller for Ag $K\alpha$ data than for Mo $K\alpha$ data (see Table 2), and since Ag $K\alpha$ radiation was used extensively for 5*d* transition-metal complexes, $K_2[MCl_6]$ (M = Re, Os, Pt). In Fig. 5(*a*) positive peaks of $+1.2\,e\,Å^{-3}$ are located on the threefold axes at 0.51 Å from the Pt nucleus and negative peaks of $-0.6\,e\,Å^{-3}$ are located on the Pt—Cl bond axis at 0.59 Å from the Pt nucleus. For the experimental map in Fig. 5(*b*), Takazawa *et al.* (1990) reported the positive peaks of $+0.9(3)\,e\,Å^{-3}$ were located at 0.46 Å from the Pt nucleus, but gave no information regarding negative peaks (estimated to be

Table 4. *Number of electrons in a sphere of the effective radius of M(Pd, Pt) for the t_{2g}, e_g, t_{1u} and a_{1g} orbitals*

Cluster	Method*	t_{2g}	e_g	$t_{2g}+e_g$	t_{1u}	a_{1g}
$[PdCl_6]^{2-}$	Calc. 1	5.53	1.90	7.43	6.29	0.24
	Calc. 2	5.51	1.95	7.46	6.29	0.26
	Calc. 3	5.54	1.91	7.45	6.29	0.24
	Calc. 4	5.51	1.97	7.48	6.29	0.25
	Calc. 5	5.47	2.07	7.54	6.29	0.26
$[PtCl_6]^{2-}$	Calc. 3	5.38	1.85	7.23	6.25	0.14
	Calc. 4	5.36	1.90	7.26	6.27	0.14
	Calc. 5	5.31	2.00	7.31	6.28	0.15

* See text for definition of Calcs. 1–5.

$-0.8\,e\,Å^{-3}$ from the contour lines in Fig. 5*b*). The calculated value of the positive peak height decreases by $0.6\,e\,Å^3$ from $[PdCl_6]^{2-}$ to $[PtCl_6]^{2-}$. This decrease is similar to the decrease of $0.5\,e\,Å^{-3}$ observed experimentally. The positive peaks given by Mo $K\alpha$ radiation have been reported to be $1.3.(8)\,e\,Å^{-3}$, which differs by only $0.1\,e\,Å^{-3}$ from that for $K_2[PdCl_6]$.

In Fig. 6 the radial charge distributions, $D(r)$s, obtained by Calc. 5 are plotted as a function of r. The differences between the $D(r)$s, $\Delta D(r)$ (Calc. 4 – Calc. 3) and $\Delta D(r)$ (Calc. 5 – Calc. 4), are depicted in Figs. 7(*a*) and (*b*), respectively. These values are similar to those in Figs. 3(*a*) and 3(*b*) for $[PdCl_6]^{2-}$. As seen in Fig. 7(*a*) the effect of the Madelung potential increases the electrons in the Pt—Cl bonding region (0.21 e) and just behind the Cl nuclei (0.07 e) by reducing those in the outer region of the cluster (0.28 e). The effect of electron correlation also increases the electrons (0.06 *e*) within the effective radius, as shown in Fig. 7(*b*).

The effective radius and effective charge given by Calcs. 3, 4 and 5 are shown in Table 1. The experimental

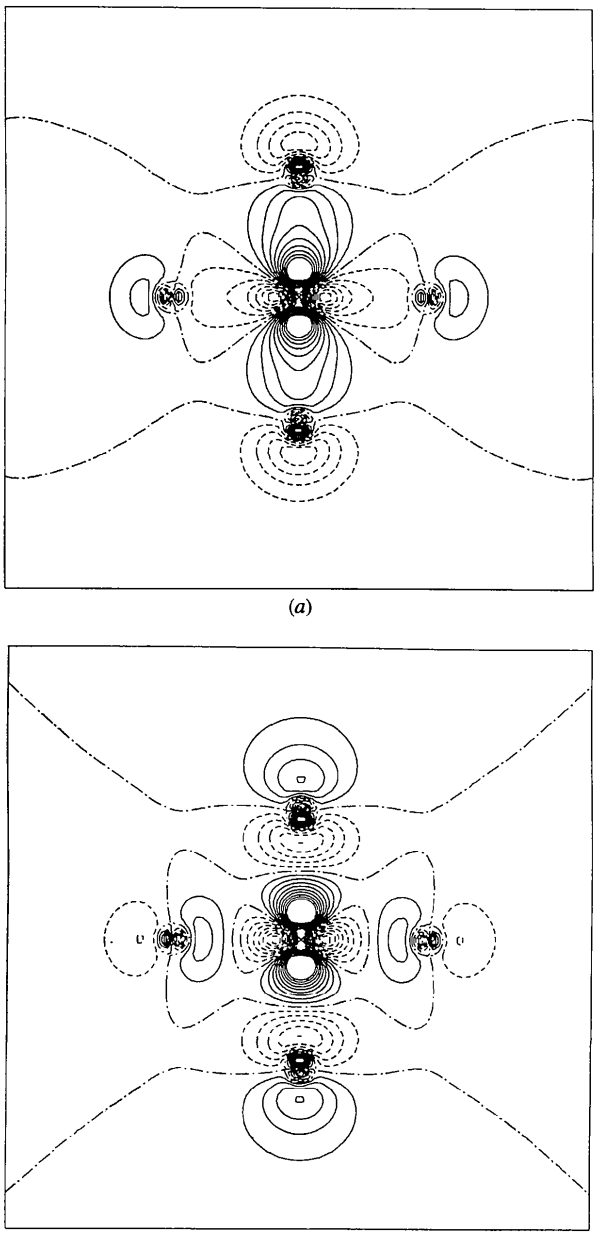

Fig. 4. (*a*) Contour map of the $2e_g$ (d_{z^2}) orbital at the xz plane given by Calc. 4 for $[PdCl_6]^{2-}$. (*b*) Contour map of the $3e_g$ (d_{z^2}) orbital (LUMO) in the xz plane given by Calc. 4 for $[PdCl_6]^{2-}$.

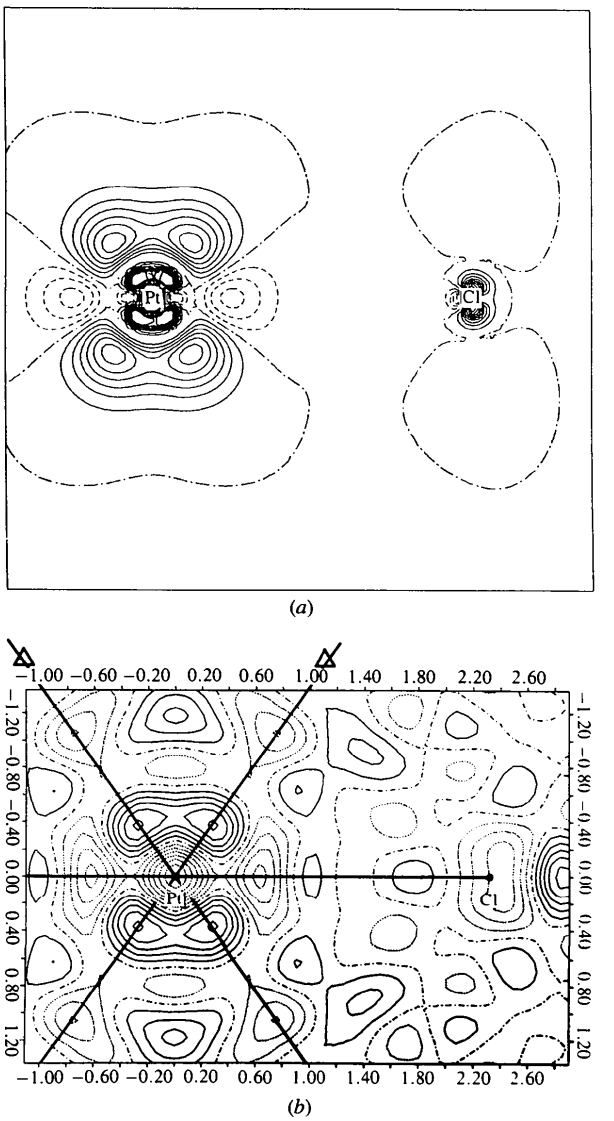

Fig. 5. (*a*) Deformation-density map in the (110) plane for $[PtCl_6]^{2-}$ given by Calc. 5. (*b*) Deformation-density map for $K_2[PtCl_6]$ at 120 K using Ag $K\alpha$ radiation (Takazawa *et al.*, 1990). Solid, broken and dash–dotted lines denote positive, negative and zero contours, respectively. Contours are drawn at intervals of $0.2\,e\,Å^{-3}$.

data obtained for $K_2[PtCl_6]$ are also given in Table 2. Calcs. 3, 4 and 5 all give almost the same effective radius of 2.30 a.u., which is larger by 0.04 a.u. than the radius of Pd. The same experimental values of 1.2 Å (2.3 a.u.) have been reported for both Pd and Pt. The effective charge of Pt is reduced by the effects of the Madelung potential and electron correlation, as with Pd (see Table 1). The effective charges of Pd and Pt given by Calc. 5 are +1.90 e and +2.27 e, respectively, implying that Pt has 0.37 e fewer electrons than Pd. Although the experimental values in Table 2 are smaller than the calculated values, both the theoretical and experimental methods give a larger effective charge for Pt than for Pd of ~0.4 e when we use the Ag $K\alpha$ data for $K_2[PtCl_6]$.

The number of electrons in a sphere of r_{so} for the t_{2g}, e_g and t_{1u} orbitals is shown in Table 3 with the r_{so} values. Calcs. 3, 4 and 5 all give essentially the same results. The r_{so} given by Calc. 5 are 2.82, 2.40 and 2.05 a.u. for the t_{2g}, e_g and t_{1u} orbitals, respectively. The r_{so} of the t_{2g} orbitals is larger than that of Pd by 0.08 a.u. and also larger than the effective radius by 0.52 a.u., whereas the r_{so} of the e_g orbitals is almost equal to that for Pd. There are almost six electrons in the t_{2g} (d_{xy}, d_{xz}, d_{yz}) orbitals and only two electrons in the e_g ($d_{z^2}, d_{x^2-y^2}$) orbitals. The number of electrons in the e_g orbitals is slightly less for Pt than for Pd. Table 4 shows the number of electrons in a sphere of the effective radius (2.30 a.u.) for the t_{2g}, e_g, t_{1u} and a_{1g} orbitals. The number of electrons in both the t_{2g} and e_g orbitals in a sphere of the effective radius decreases from Pd to Pt. These decreases in the d electrons cause Pt to have a greater effective charge than Pd (see Table 1), as discussed above. The experimental value for the electron populations in the ($t_{2g} + e_g$) orbitals given in Table 2 increases from Pd to Pt, which contrasts with our present calculated results. The increase in electrons in these orbitals is also not consistent with the increase in the effective charge from Pd to Pt shown in Table 2. The differences in the effective radius and the d-electron distribution between Pd and Pt can be attributed to the diffuse $5d$ orbitals of the Pt atom, compared with the $4d$ orbitals of the Pd atom. The characteristics of the molecular orbitals are essentially the same as those of $[PdCl_6]^{2-}$. However, the bonding nature of the $2e_g$ orbitals is stronger in $[PdCl_6]^{2-}$

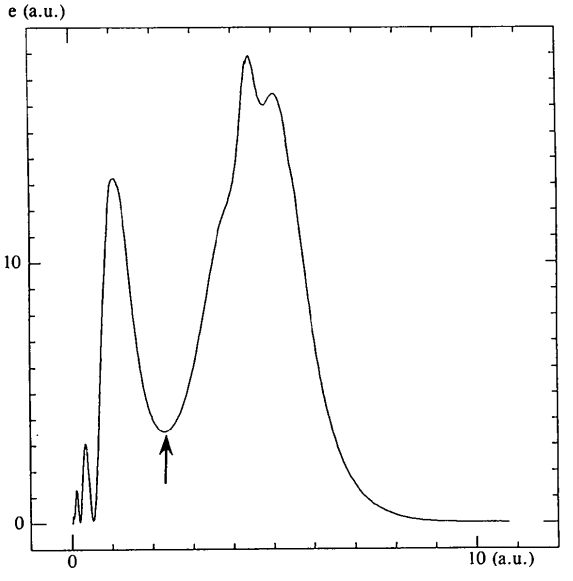

Fig. 6. Radial charge distribution, $D(r)$, given by Calc. 5 for $[PtCl_6]^{2-}$. The arrow indicates the position of the effective radius.

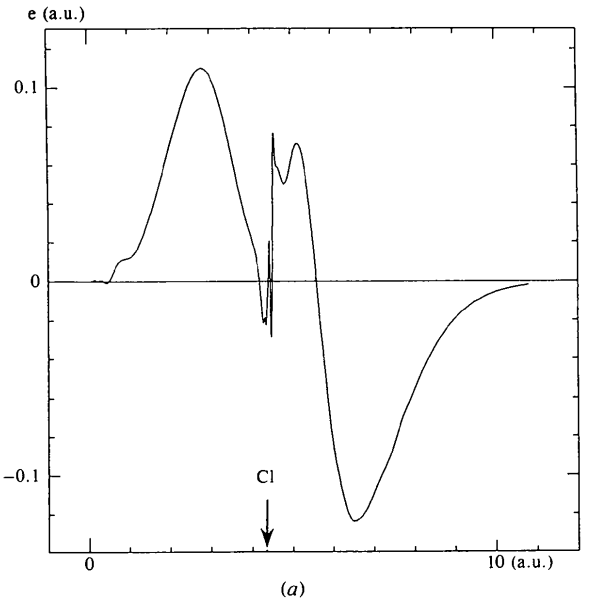

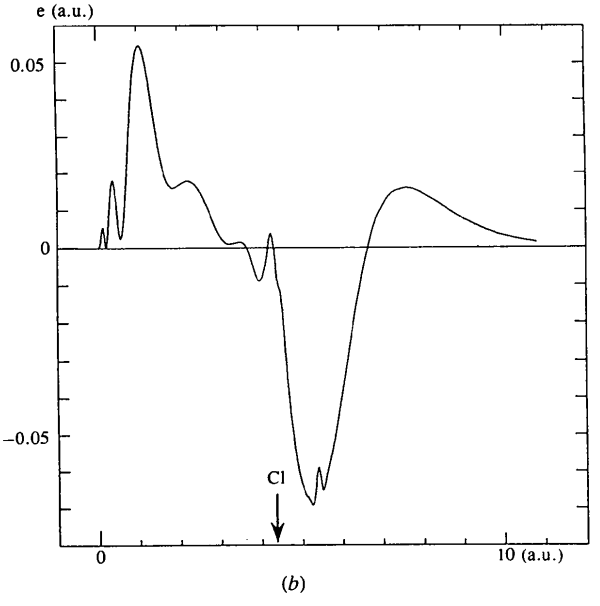

Fig. 7. (*a*) Difference in $D(r)$, $\Delta D(r)$ (Calc. 4 – Calc. 3), for $[PtCl_6]^{2-}$. (*b*) Difference in $D(r)$, $\Delta D(r)$ (Calc. 5 – Calc. 4), for $[PtCl_6]^{2-}$.

than in $[PtCl_6]^{2-}$. In fact, the M—Cl overlap population given by Calc. 5 increases from 0.33 e for $[PtCl_6]^{2-}$ to 0.51 e for $[PdCl_6]^{2-}$.

4. Concluding remarks

The charge asphericity caused by the d electrons observed for $K_2[PdCl_6]$ and $K_2[PtCl_6]$ crystals was analyzed using theoretical calculations. HF and SDCI calculations were performed for $[PdCl_6]^{2-}$ and $[PtCl_6]^{2-}$ with and without taking into account the Madelung potentials. Model potentials (MPs) were used to replace the core electrons of atoms. Major relativistic effects were incorporated into the MPs for Pd and Pt. For Cl atoms, we examined both the all-electron (AE) and MP calculations to verify the validity of using the MP. We found that the MP method works very well and enables us to observe the fine structure of the valence electron distribution within a cluster. Although the charge asphericity can essentially be explained using calculations based on the bare cluster model, the effects of the Madelung potential and electron correlation increase the electron inside the cluster, which strengthens the M—Cl bonds.

The deformation-density maps in the (110) plane given by our calculations are quite similar to the experimental results reported by Takazawa *et al.* (1988, 1990). The effective charges and effective radii of Pd and Pt, and the number of electrons in the t_{2g}, e_g and t_{1u} orbitals were calculated by direct integration. Our theoretical results suggest that the positive peaks on the threefold axes and the negative peaks on the M—Cl bond axis in the deformation densities maps correspond to the excess d electrons ($4d$ of Pd and $5d$ of Pt) in the t_{2g} (d_{xy}, d_{xz}, d_{yz}) orbitals and the electron deficiency in the e_g (d_{z^2}, $d_{x^2-y^2}$) orbitals, respectively. The calculated value of the positive peak height decreases by 0.6 e Å^{-3} from $[PdCl_6]^{2-}$ to $[PtCl_6]^{2-}$. This decrease is consistent with the decrease of 0.5 e Å^{-3} found experimentally.

The effective radii for M atoms were calculated to be 2.26 and 2.30 a.u. for $[PdCl_6]^{2-}$ and $[PtCl_6]^{2-}$, respectively, which were comparable to the experimental value of 1.2 Å (2.3 a.u.) obtained for both $K_2[PdCl_6]$ and $K_2[PtCl_6]$. The number of electrons in a sphere of the effective radius of M was smaller for $[PtCl_6]^{2-}$ than for $[PdCl_6]^{2-}$, resulting in a larger effective charge for Pt (+2.27 e) than for Pd (+1.90 e). Although the absolute values of the effective charges obtained experimentally are smaller than the calculated values, the difference in the experimental values for the two systems (M = Pt and Pd) is similar to the calculated value (0.4 e).

Generally, it is difficult to obtain a deformation-density map for a system such as the $K_2[PtCl_6]$ crystal by the X-ray diffraction method, due to the very small valence/total electron ratios. On the other hand, we can obtain theoretical deformation-density maps without any ambiguity, since the charge densities of both cluster and component atoms can be calculated using the same basis sets. In addition, the relativistic effects can be incorporated effectively in our model potentials and basis sets. Thus, molecular orbital calculations using the model potential method are quite useful for explaining the aspherical distribution of d electrons in the ligand field.

The authors would like to thank Professor Shigeru Ohba of Keio University for allowing us to use his experimental results. This study was supported in part by a Grant-in-Aid for Scientific Research on Priority Areas (Theory of Chemical Reactions) from the Ministry of Education, Science and Culture.

References

Buenker, R. J. & Peyerimhoff, S. D. (1974). *Theor. Chim. Acta*, **35**, 33–58.

Coppens, P. & Hall, M. B. (1982). Editors. *Electron Distributions and the Chemical Bond*. New York: Plenum Press.

Cowan, R. D. & Griffin, D. C. (1976). *J. Opt. Soc. Am.* **66**, 1010–1014.

Gershgorn, Z. & Shavitt, I. (1968). *Int. J. Quantum Chem.* **2**, 751–759.

Huzinaga, S., Andzelm, J., Klobukowksi, M., Radzio-Andzelm, E., Sakai, Y. & Tatewaki, H. (1984). *Gaussian Basis Sets for Molecular Calculations*. Amsterdam: Elsevier.

Johansen, H. (1976). *Acta Cryst.* A**32**, 353–355.

Kashiwagi, H., Obara, S., Takada, T., Sasaki, F. & Miyoshi, E. (1979). *JAMOLA Program Package for HF Calculations*.

McLean, A. D. & Liu, B (1973). *J. Chem. Phys.* **58**, 1066–1078.

Miyoshi, E. (undated). *JANIE Program Package for Numerical Integration of Charge Density*.

Miyoshi, E. & Sakai, Y. (1988*a*). *J. Comput. Chem.* **9**, 719–727.

Miyoshi, E. & Sakai, Y. (1988*b*). *J. Chem. Phys.* **89**, 7363–7366.

Miyoshi, E., Sakai, Y. & Katsuki, S. (1991). *Surf. Sci.* **242**, 531–537.

Murakami, A., Iwaki, H., Terashima, H., Shoda, S., Kawaguchi, T. & Noro, T. (undated). *MICA3 Program Package for CI Calculations*.

Ohba, S. & Saito, Y. (1984). *Acta Cryst.* C**40**, 1639–1641.

Ohba, S., Sato, S., Saito, Y., Ohshima, K. & Harada, J. (1983). *Acta Cryst.* B**39**, 49–53.

Sakai, Y. & Huzinaga, S. (1982*a*). *J. Chem. Phys.* **76**, 2537–2551.

Sakai, Y. & Huzinaga, S. (1982*b*). *J. Chem. Phys.* **76**, 2552–2557.

Sakai, Y. & Miyoshi, E. Unpublished work.

Sakai, Y. & Miyoshi, E. (1987). *J. Chem. Phys.* **87**, 2885–2892.

Sakai, Y. & Miyoshi, E. (1988). *J. Chem. Phys.* **89**, 4452–4453.

Sakai, Y., Miyoshi, E., Klobukowski, M. & Huzinaga, S. (1987*a*). *J. Comput. Chem.* **8**, 226–255.

Sakai, Y., Miyoshi, E., Klobukowski, M. & Huzinaga, S. (1987*b*). *J. Comput. Chem.* **8**, 256–264.

Sano, M., Hatano, Y., Kashiwagi, H. & Yamatera, H. (1981). *Bull. Chem. Soc. Jpn,* **54**, 1523–1530.

Sano, M., Kashiwagi, H. & Yamatera, H. (1982). *Inorg. Chem.* **21**, 3837–3841.

Stevens, E. D. & Coppens, P. (1976). *Acta Cryst.* A**32**, 915–917.

Takazawa, H., Ohba, S. & Saito, Y. (1988). *Acta Cryst.* B**44**, 580–585.

Takazawa, H., Ohba, S., Saito, Y. & Sano, M. (1990). *Acta Cryst.* B**46**, 166–174.

Tatewaki, H., Tanaka, K., Sasaki, F., Obara, S., Ohno, K. & Yoshimine, M. (1979). *Int. J. Quantum Chem.* **15**, 533–545.

Toriumi, K. & Saito, Y. (1983). *Advances in Inorganic Chemistry and Radiochemistry,* pp. 27–81. New York: Academic Press.